land

MDPI

Article

Mercury Content in Volcanic Soils of Isla Santa Cruz (Galápagos, Ecuador)

Antonio Martínez Cortizas [1,2,*], Ainé Francos-Golán [3,4,*], Mohamed Traoré [5], Jenny Kristina Sjöström [3,4] and Olalla López-Costas [3,4]

1 EcoPast (GI-1553), Facultade de Bioloxía, Universidade de Santiago de Compostela, 15782 Santiago de Compostela, Spain
2 Bolin Center for Climate Research, Stockholm University, 10691 Stockholm, Sweden
3 EcoPast (GI-1553), Cross-Disciplinary Research Center on Environmental Technologies (CRETUS), Área de Arqueoloxía, Departamento de Historia, Universidade de Santiago de Compostela, 15782 Santiago de Compostela, Spain; jennykristina.sjostrom@usc.es (J.K.S.); olalla.lopez@usc.es (O.L.-C.)
4 Archaeological Research Laboratory, Stockholm University, Wallenberglaboratoriet, 10691 Stockholm, Sweden
5 Advanced Materials Department, Fundación Cenrtro Tecnológico de Investigación Multisectorial (CETIM), 15180 Culleredo, Spain; traore.mohamed19@gmail.com
* Correspondence: antonio.martinez.cortizas@usc.es (A.M.C.); aine.francos.golan@usc.es (A.F.G.)

Abstract

Mercury is closely associated with volcanic environments such as Islas Galápagos. Isla Santa Cruz, one of the oldest Galápagos islands, has undergone intense land-use transformations that have likely affected mercury cycling. A pre-transformation mercury baseline is approached here with a unique collection of 40 soil profiles (114 samples) collected in 1962 during the geopedological survey performed by researchers at Ghent University (Belgium). The influence of soil properties and bioclimatic conditions is assessed by combining mercury analysis, vibrational spectroscopy, elemental analyses (Fe), and chemical weathering data, using covariation analysis and structural equation modeling (SEM). In the 1960s, Isla Santa Cruz soils were enriched in mercury (36–679 ng g^{-1}) with concentrations in line with those of other volcanic soils, but no differences between topsoils and subsoils were found. Mercury content correlated with soil components (organic matter, Fe) and degree of chemical weathering. The SEM model (R^2 0.87, SRMR 0.09) indicated that primary minerals (negative) and altitude (positive) have the largest controls, suggesting that bioclimatic conditions and mineral weathering drive the mercury spatial distribution. Our results establish a reference state for Isla Santa Cruz, and additional research may help to understand the potential impacts of land-use changes on the mercury cycle in the island.

Keywords: volcanic soils; Galapagos Islands; mercury; soil properties; structural equation modeling

Check for updates

Academic Editor: Nick B. Comerford

Received: 29 August 2026
Revised: 26 September 2026
Accepted: 29 September 2026
Published: 9 October 2026

Copyright: © 2026 by the authors. Licensee MDPI, Basel, Switzerland. This article is an open access article distributed under the terms and conditions of the Creative Commons Attribution (CC BY) license.

1. Introduction

Isla Santa Cruz is geologically one of the oldest islands of the Galapagos archipelago with the highest population concentration and the largest area of human-impacted soils [1]. The archipelago is situated in an active volcanic region, but Isla Santa Cruz is located on the remnants of non-active volcanoes [2]. The local geology is primarily characterized by volcanic rocks, consisting of magnesium-rich alkaline basalts with aphanitic and plagioclase-porphyritic structures, associated with interbedded submarine sediments [3,4]. The characteristics of soils of Isla Santa Cruz primarily derive from the weathering of relatively recent pyroclastic deposits at different altitudes, climatic conditions, and vegetation

composition. These variations result in an altitudinal soil distribution defined by distinct bioclimatic zones [2]: the high altitude, very humid, and temperate zone is characterized by Andisols; the intermediate altitude, wet, and warm zone contains Inceptisols and Alfisols; and the low elevation, dry to very dry warm zone consists of Alfisols, Mollisols, and Entisols [5].

The existing body of research on the soils of Isla Santa Cruz has focused on identifying the processes governing local pedogenic development. The main factors controlling pedogenesis are climate and altitude [6]. For instance, the evaluation of different weathering indices revealed that soils at higher altitudes in humid zones are significantly more weathered than those at low elevations in arid coastal areas [7,8]. Similarly, key soil parameters—such as secondary Al, Fe, and Si contents or soil organic carbon (SOC) stocks—appear to be strongly governed by these climatic and altitudinal conditions [9,10]. However, physical properties of parent materials also modulate these effects; specifically, there is evidence that high-porosity scoria is subject to accelerated weathering compared to dense lava, although the latter parent material supports thicker soil formation [11–13]. Additionally, under humid conditions, soil age serves as a critical determinant of physicochemical and microstructural evolution across the soil developmental sequence, with progressive weathering marked by decreasing pH, electrical conductivity, soil organic carbon, cation exchange capacity, and water retention alongside increasing clay content and bulk density [14–16]. Furthermore, recent studies on heavy metal retention dynamics reveal that soil sorption capacity for copper and cadmium correlates with elevation gradients yet decreases with soil age—with the youngest soils exhibiting the highest retention capacity [17,18].

Volcanic regions represent an important natural source of mercury to the atmosphere, but mercury concentrations in volcanic soils reflect both geogenic inputs from parent material and mercury deposited from the atmosphere [19–21]. In volcanic soils, total mercury commonly decreases with depth and is strongly influenced by soil organic matter, as well as by Al- and Fe-bearing phases that can enhance its retention during soil development [21–25]. Because part of the mercury stored in these soils may be inherited from volcanic parent material, conservative lithogenic elements such as Al, Ti, Zr, and Sc have been used to distinguish lithogenic from externally supplied mercury [24–26]. Studies of volcanic soils further indicate that pedogenic processes, including weathering, formation of metal–humus complexes, and accumulation of poorly crystalline Al and Fe phases, can substantially modify its distribution and retention [21,24]. In addition, changes in climate, vegetation, land use, and fire regimes can alter terrestrial mercury inputs, storage, and remobilization, potentially changing both the magnitude of mercury stored in soils and its subsequent release to the atmosphere and other environmental pools [27,28], posing poorly constrained health risks to humans and ecosystems.

On Isla Santa Cruz, major changes in vegetation cover and land use occurred during the last six decades. In 1961, 94% of unprotected areas were covered by native vegetation, compared with only 7% in 2018, following extensive agricultural expansion [29]. These profound land-cover changes, together with ongoing climate change, have the potential to alter the biogeochemical soil conditions controlling mercury retention and mobilization. In this investigation, we take advantage of a unique collection of archived soil samples collected in 1962, during a Belgian (Ghent University) geopedological survey, prior to most of the documented land-cover transformations, to investigate the processes controlling mercury distribution under largely pre-transformation conditions. Establishing this baseline provides a foundation for future assessment of how subsequent land-use and vegetation changes have affected mercury dynamics in volcanic soils on Isla Santa Cruz. In this investigation, we aimed to determine the role of soil components, chemical weathering, and environmental conditions (i.e., bioclimatic zones) in the spatial and vertical changes in

mercury soil content, through the application of statistical modeling (structural equation modeling, SEM).

2. Material and Methods

2.1. Location, Bioclimatic Zones, and Sampling

Isla Santa Cruz is located in the Galapagos Archipelago (Ecuador) (Figure 1). The geographical and geological context of the island has been described in detail in previous publications [8,9]. Generally, the geology is composed of marine sediments covered by volcanic materials formed by tholeiitic and alkaline basalts [30], which were characterized as lava flows, scoria, and ash (tephra) deposits [6]. As summarized by Wilson et al. [31], the oldest volcanic materials (Platform Series) were emplaced between 1.62 and 1.16 Ma, while the more recent materials (Shield Series) were emplaced between 271 and 74 ka. From the coastal platform to the higher elevations (Cerro Crocker, 855 m a.s.l.), an intense rainfall gradient (500–2000 mm) develops in the windward slopes of the island, favored by the trade winds and oceanic currents [32,33]. This gradient determines contrasted changes in bioclimatic conditions with elevation configuring five main zones [34,35]: the arid zone (AZ, <100 m a.s.l.), the transition zone (TZ, 100–240 m a.s.l.)), the Scalesia zone (SZ, 240–400 m a.s.l.), the brown zone (BZ, 400–500 m a.s.l.), and the Miconia/Upland zone (MZ, >500 m a.s.l.). As indicated in the introduction, at low altitude, Entisols, Alfisols, and Mollisols predominate, Inceptisols and Alfisols predominate at intermediate altitude, and Andisols predominate at high altitudes [5].

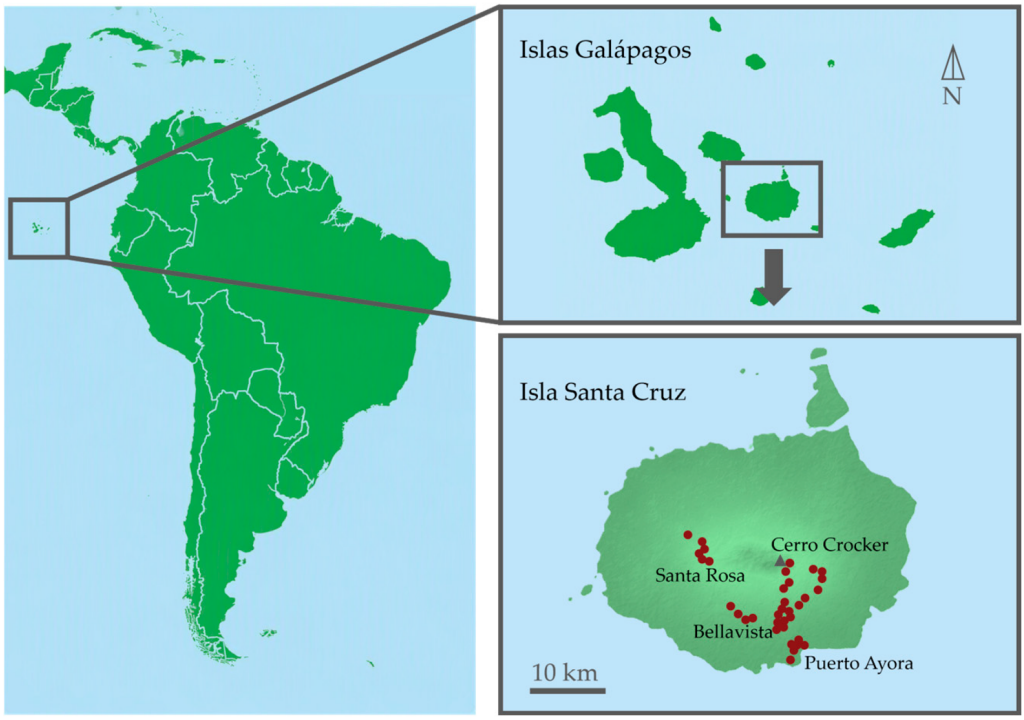


Figure 1. Map of Islas Galápagos indicating the position of Isla Santa Cruz in the center of the archipelago with the approximate location of the sampling soils, based on Stoop et al. [6,7]. The read dots correspond to the sampling sites. The figure was created by the authors using IA for color transformation and Wikipedia for map-based forms.

The soils were sampled on the windward slopes of the island in 1962, in the context of a Belgian (Ghent University) geopedological survey. A detailed soil description, based on the field notes of the Belgian survey, can be found in Taboada et al. [8]—also in the Supplementary Materials of that publication. In this study, we used 40 of the sampled soils

(114 samples): 7 soils from the AZ (16 samples), 16 soils from the TZ (52 samples), 9 soils from the SZ (26 samples), and 9 soils from the BZ (20 samples). No soils were sampled in the MZ. Here, we use the term "topsoil" to refer to soil samples that were originally coded as A horizons, and "subsoil" for those coded as B or C horizons (see Supplementary Materials in [8]).

The original soil samples were stored in a cool, dry, dark place at Ghent University (Belgium). In 2006, the soil collection was subsampled, under the supervision of Prof. Georges Stoops and in agreement with one of the co-authors (AMC). Samples were taken to the Soil Science Department of Universidade de Santiago de Compostela (Spain), dried at 35 °C for two weeks and subsequently milled (using a Retsch MM101 mill) to very fine powder (<50 μm), and kept in sealed Eppendorf tubes, in a dry, cool, dark place under our (AMC) supervision.

2.2. Data from Previous Investigations

In volcanic soils, mercury is mainly associated with organic matter and iron compounds. Chemical weathering results in the formation of highly reactive compounds—both crystalline and of low crystallinity. Thus, for this investigation, we used data on Fe content, as well as chemical weathering indices obtained from the Supplementary Materials of a previous investigation [8–10]. As four of the chemical indices were highly correlated [8], here we selected data for two of them: the weathering index of Parker (WIP) and the silica–titania index (STI). These two indices are well-established bulk-geochemical parameters used to quantify the intensity of chemical weathering and elemental mobility in rock-to-soil chronosequences [36]. Specifically, WIP assesses the loss of mobile alkali and alkaline earth cations relative to their oxygen bond strengths because it tracks the depletion of basic cations during weathering, and its value decreases as the degree of weathering increases. Values lower than 20 are taken as an indication of strong weathering intensity. STI assesses the degree of desilication relative to immobile titanium dioxide accumulation during advanced chemical alteration [37]. In volcanic soils, the rapid chemical weathering also implies the release and loss of Si; thus, the STI accounts for this process, and the values decrease as weathering intensity increases [8].

2.3. Mercury Analysis

Total mercury concentrations were determined using a DMA-80 analyzer (Milestone^{TM} SpA, Sorisole, Italy), which combines thermal decomposition and gold-trap amalgamation with cold-vapor atomic absorption spectrometry (CV-AAS). The instrument is housed within the EcoPast Research Group facilities at the CRETUS Institute, Universidade de Santiago de Compostela, Spain. Approximately 25 mg of homogenized sample was weighed for each measurement. Analytical quality assurance and quality control procedures included the analysis of two certified reference materials (CRMs), one procedural blank every two samples, and sample replicates. The CRMs comprised NIST SRM 1547 (Peach Leaves; certified Hg concentration: 31 ± 4 ng g^{-1}) and BCR-277R (Estuarine Sediment; certified Hg concentration: 128 ± 17 ng g^{-1}), yielding recoveries of 105.6% and 104.2%, respectively. Duplicate analyses were performed for 33% of the samples, with a mean coefficient of variation of 5%. The method detection limit was 3.3 ng g^{-1}.

Studies conducted on archived soils have shown that mercury concentrations in mineral and organic soils are stable even after long storage times [38]. This is consistent with the strong binding of mercury to soil components, as is discussed in Section 4.1.

2.4. Vibrational Spectroscopy (FTIR-ATR)

Before the mercury analysis, all samples were analyzed by vibrational spectroscopy in the Mid-infrared (MIR) range (4000–400 cm^{-1}). Spectra were acquired using an FTIR-ATR

instrument (Fourier Transform Infrared—Attenuated Total Reflectance) (Cary 630, Agilent Technologies Inc., Santa Clara, CA, USA), located at the EcoPast Research Group laboratory, Faculty of Biology, Universidade de Santiago de Compostela, Spain. Spectra were recorded at a resolution of 4 cm^{-1}, averaging 100 scans per sample to maximize spectral quality and reduce the signal-to-noise ratio. Spectral processing was conducted with Orange Data Mining software v3.39.0, including baseline correction and standardization [39]. FTIR-ATR provides information simultaneously on inorganic and organic components.

2.5. Statistical Methods

Covariation between elements (Fe, Hg) and weathering indices was assessed by correlation analysis (i.e., Pearson "r" coefficient). To determine the main factors involved in mercury content in these soils, we applied structural equation modeling (PLS-SEM) using SmartPLS software (version 4.1.1.5) [40]. PLS-SEM enables the use of several proxies for each latent variable (LV, both predictors and response) and avoids multicollinearity. PLS-SEM requires a relatively low sample size; it is very efficient with non-normal distributions and is adequate for explanatory and predictive purposes. In the models, proxies for the LV were retained only when their loadings were 0.9 or greater. Direct effects of the predictors on the response latent variable (i.e., Hg), as well as interactions between predictors (i.e., indirect effects), are also calculated. The sum of direct and indirect effects determines the total effect, providing a weight value for each predictor on the response variable. As a first step to define the SEM model, we calculated the correlation between mercury and absorbances for each wavenumber (i.e., correlation spectrum with "r" Pearson coefficients; see Section 3.3 below). MIR regions of the spectrum showing moderate-to-large positive and negative correlations with mercury were selected for the model, together with supporting data on elemental composition and weathering indices (Fe, WIP, and STI). To check the validity of the model, the SmartPLS bootstrapping function was used so path coefficients and total effects of the predictor LVs were only retained when found to be significant ($p < 0.05$).

3. Results

Here we first briefly describe elemental (Fe content) and chemical weathering (WIP and STI) data from previous investigations, followed by presentation of the new data obtained within this study (MIR data and Hg data).

3.1. Iron and Weathering Indices

Iron concentrations showed large variations (Figure 2). The lowest values were found in soils from AZ, and the largest in soils from BZ; the soils from TZ and SZ showed intermediate values. Significant differences ($p < 0.001$) between bioclimatic zones were found for topsoils and subsoils. For topsoils, the sequence was as follows: AZ < TZ = SZ < BZ; and for subsoils, the sequence was as follows: AZ < TZ < SZ = BZ. No significant ($p = 0.07$) differences between topsoils and subsoils were found. Iron was correlated with altitude, but the correlation was higher for subsoils (Table A1).

The intensity of chemical weathering followed a similar pattern to Fe, with increasing intensity with altitude. Greater variability was found for WIP, which reflects depletion of basic cations, than for STI, which is related to Si mobility in volcanic soils. These indices showed no significant differences between topsoils and subsoils ($p = 0.167$ and $p = 0.983$, respectively). WIP and STI also showed significant differences between bioclimatic zones for topsoils ($p < 0.001$) and subsoils ($p < 0.001$), with the following sequences: BZ < TZ = SZ = AZ, WIP in topsoils; BZ = SZ = TZ < AZ, WIP in subsoils; BZ < SZ = TZ < AZ, STI in topsoils; and BZ < SZ < TZ < AZ, STI in subsoils, respectively. Correlation between these chemical weathering indices was not significant for topsoils and only moderate for subsoils (Table A1).

Both indices were negatively correlated with Fe, meaning that increased chemical weathering is accompanied by increases in iron content. Despite this, STI was not significantly correlated with Fe in topsoils. Again, correlation coefficients were higher for subsoils.

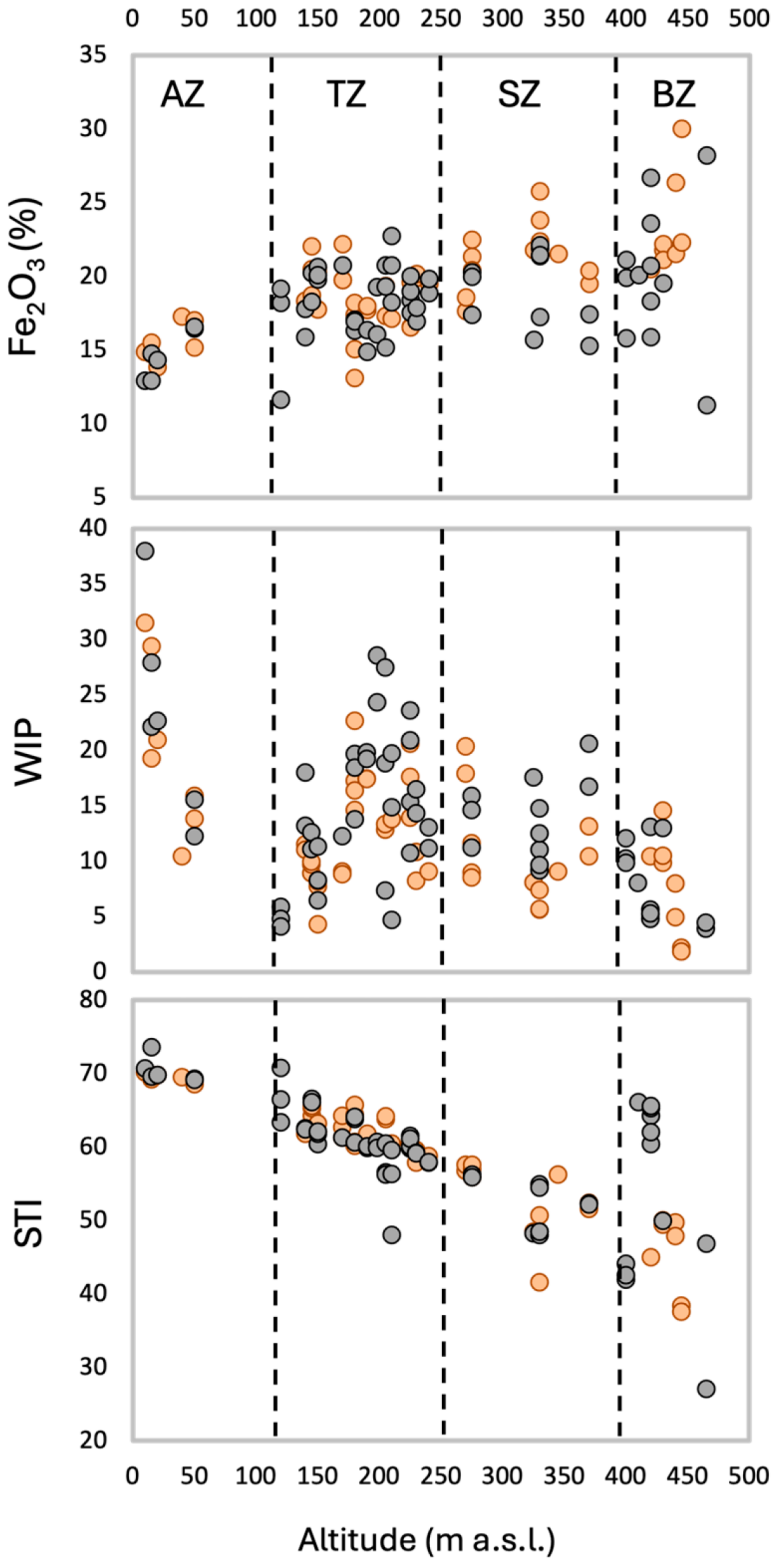


Figure 2. Altitudinal variations in iron (%) content and chemical weathering indices (WIP, weathering index of Parker; STI, silica–titania index). Topsoils (A horizons), grey circles; subsoils (B and C horizons), orange circles. Bioclimatic zones: AZ, arid zone; TZ, transition zone; SZ, Scalesia zone; BZ, brown zone (after [34,35]). Data obtained from Taboada et al. [8].

3.2. Mid Infrared (MIR) Vibrational Spectroscopy Characterization

The MIR spectra of the topsoil and subsoil samples, grouped by bioclimatic zone, are represented in Figure 3. The spectra are quite similar but also show some differences between bioclimatic zones. Intense absorbance was found in the 1200–800 cm^{-1} region, moderate absorbance in the 3800–2800 cm^{-1} and 600–400 cm^{-1} regions, weak to moderate absorbances in the 1800–1300 cm^{-1} region, and very weak absorbances in the 800–600 cm^{-1} region. Most absorbances can be assigned to clay minerals: kaolinitic clay (kaolinite and halloysite), gibbsite, smectite, and probably talc (Table A2). Kaolinitic clay is present in all soils, regardless of the bioclimatic zone, although the typical OH vibrations in the 3700–3600 cm^{-1} region tend to decrease from the TZ to the BZ and from topsoils to subsoils (Figure 3). Gibbsite was only found in soils from SZ and BZ, with its typical absorbances better expressed in topsoils than in subsoils—in the BZ in particular. Variations in smectite and talc content are more difficult to assess since vibrations of these clays overlap both with those of kaolinitic clay and gibbsite. Distinguishing these minerals requires further studies and is part of an ongoing investigation.

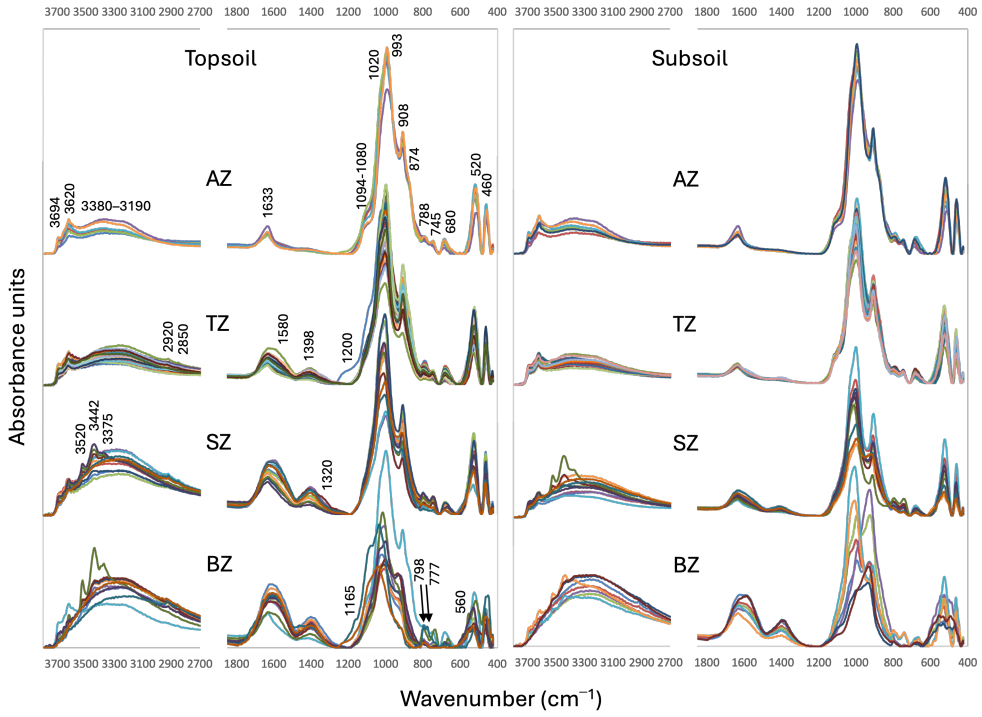


Figure 3. Spectra of the analyzed soil samples ordered by bioclimatic zone, with indications of wavenumbers of some of the main absorbances. Colors are used with the purpose to enhance visualization. Bioclimatic zones: AZ, arid zone; TZ, transition zone; SZ, Scalesia zone; BZ, brown zone (after [34,35]).

A more detailed inspection of the spectra using second derivative analysis also suggested the presence, in low amounts, of primary silicates as plagioclase (anorthite), Na-feldspar (albite), olivine (most likely fayalite), pyroxene (augite, diopside, and enstatite), and quartz (Table A2). Quartz was only identified (1165, 798, 777 cm^{-1}) in soils of the SZ and BZ. Clay adsorbed water (1633 cm^{-1}) was present in all samples, and this band broadened and increased in absorbance from the AZ to the BZ, accompanied by an increase in the band centered at 1400 cm^{-1}. Second derivative spectra also showed a greater diversity of vibrations, corresponding to aliphatics (2960, 2920, 2850, 1400–1250 cm^{-1}), carbonyl (1730–1720 cm^{-1}), carboxylic (1700–1680 cm^{-1}), and aromatic (1650–1550 cm^{-1}) bonds, all

assigned to organic matter (OM) compounds. The increase in OM vibrations is evident in the topsoils and less so in the subsoils, with the exception of the soils on the BZ.

3.3. Mercury Content

Mercury concentrations varied by an order of magnitude, from a minimum of 36.4 ng g^{-1} to a maximum of 678.8 ng g^{-1}. Average concentrations in topsoils and subsoils increased from the AZ to the SZ and stabilized at the BZ (Table 1). Differences for both soil compartments (i.e., topsoils and subsoils) were highly significant ($p < 0.001$): AZ < TZ < SZ = BZ. Nevertheless, mercury concentrations in samples taken at increasing depths were highly correlated with those of the upper soil sample (r 0.93–0.97, $p < 0.001$; Figure A1).

Table 1. Average (avg), standard deviation (std), minimum (Min), and maximum (Max) mercury concentrations in topsoil and subsoil samples of soils of Isla Santa Cruz, by bioclimatic zone. AZ: arid zone; TZ: transition zone; SZ: Scalesia zone; BZ: brown zone (after [34,35]).

Topsoil	**AZ**	**TZ**	**SZ**	**BZ**
Avg ± std	48.0 ± 5.7	281 ± 121.9	504.0 ± 53.8	514.3 ± 130.5
Min–Max	42.7–57.4	92.0–458.4	414.0–567.7	290.2–678.8
N	6	33	12	12
Subsoil				
Avg ± std	56.9 ± 13.5	235.6 ± 113.5	487.7 ± 97.6	494.4 ± 112.2
Min–Max	36.4–80.4	56.7–442.7	332.2–643.3	322.5–628.4
N	7	26	12	8

Figure 4 shows that mercury concentrations increase with altitude, following a pattern that can be fitted to a quadratic function (r = 0.87, $p < 0.01$). Mercury was also correlated with iron content (topsoil r = 0.53, $p < 0.01$; subsoil r = 0.72, $p < 0.01$) and degree of chemical weathering (STI, topsoil r = −0.75, $p < 0.01$; subsoil r = −0.85, $p < 0.01$) (see also Table A1).

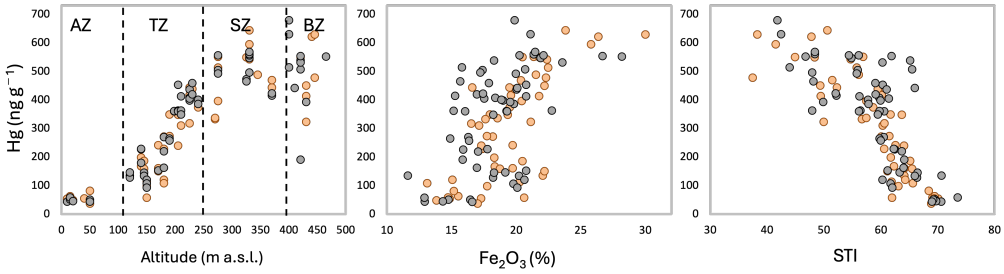


Figure 4. Mercury content in the soils of Isla Santa Cruz; relationship to altitude, iron content, and chemical weathering (STI). Grey circles: topsoils (A horizons); orange circles: subsoils (B and C horizons). Bioclimatic zones: AZ, arid zone; TZ, transition zone; SZ, Scalesia zone; BZ, brown zone (after [34,35]).

MIR absorbances also showed large positive and negative correlations to mercury content (Figure 5), and the shape of the correlation spectra is almost identical for topsoils and subsoils. Large positive correlations were found for the 3400–2800 cm^{-1} region (maxima, r > 0.80, in the 3090-2965 cm^{-1} region; Figure A2), in the 1700–1340 cm^{-1} region (r > 0.70), and at 587 and 477 cm^{-1}. Most of these vibrations can be related to aliphatic, carbonyl, carboxylic, and aromatic bonds of the soil organic matter. Moderate to large negative correlations were found in the 1130–600 cm^{-1} region (minima at 1122, 962, 868, 822, 784, 766, 706, 684, and 641 cm^{-1}), and at 503 and 453 cm^{-1} (Figure A2). Negative correlations are related to both secondary (kaolinitic clay, gibbsite, and smectite) and primary (olivine, pyroxene, feldspar, and plagioclase) silicates (Table A2).

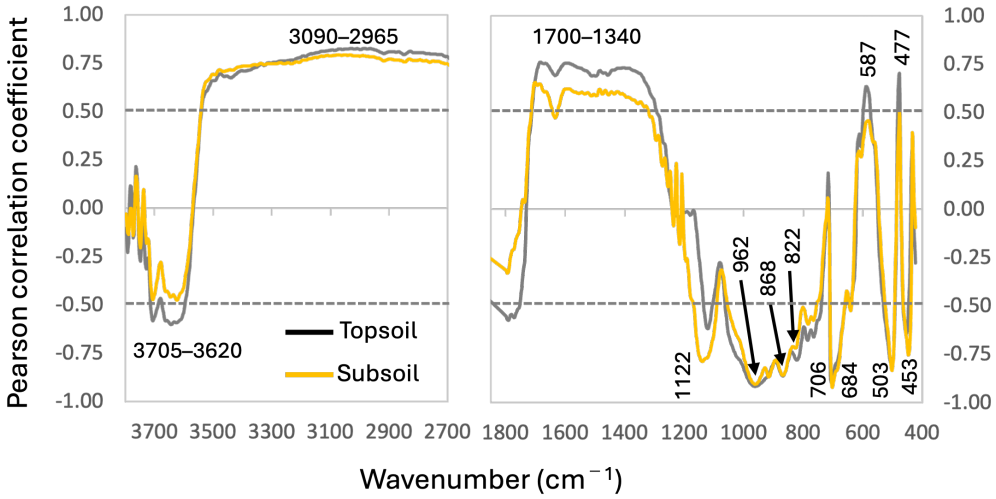


Figure 5. Correlation spectrum of mercury concentrations with MIR absorbances in topsoil and subsoil samples. Wavenumbers of absorbances with high correlation (positive: >0.5; negative: <−0.5) are also indicated.

3.4. Structural Equation Modeling (SEM) of Soil Mercury Content

Next, we build a SEM model using mercury content as a latent response variable (LV) and selected soil properties as predictor LVs (clay, iron, organic matter, and primary mineral content together with soil weathering indices, and altitude—the inner model). As indicated in Section 2, we iterated the model and, in each run, eliminated those components and interactions (i.e., paths) that were not significant after bootstrapping analysis. In the final model, the following LVs were retained: altitude, degree of weathering, primary minerals, and soil organic matter content (Figure 6A). Each of the LVs were represented by one or more proxies (the outer model), which were retained only if their loadings were greater than 0.9: altitude (Alt), log-transformed to account for the non-linearity of the relationship to mercury; degree of chemical weathering (Weath), Fe content, and STI; primary minerals (Pmin) and MIR vibrations (960, 864, 823, 701, 684, and 501 cm^{-1}); and organic matter compounds (OM) and MIR vibrations of organic compounds (3090, 2922, 2911, 2855, 1700, 1661, 1590, 1463, 1439, 1420, 1405, and 1377 cm^{-1}).

The model was run for the full set of samples (complete model, Figure 6A) and for the topsoils and subsoils separately (segregated models, Figure A3). The complete model explained 87% (R^2 0.87, SRMR 0.09) of the variance of soil mercury concentrations (Figure 6B). Alt showed a large significant interaction with OM and a large negative interaction with Weath, and a low interaction with Pmin (Figure 6A). OM showed a moderate negative interaction with Weath but a large negative interaction with Pmin. Interactions between predictor LVs accounted for 88% of the variance in Pmin, 59% of the variance of Weath, and 40% of the variance of OM. The path coefficients suggest that the largest direct, negative effect on mercury concentrations was exerted by Pmin, followed by OM content, and Weath. Alt had only a minor direct effect on soil mercury concentrations. Total effects, which account for the direct and indirect effects (i.e., controls due to interactions between predictors), also indicate that the largest negative effect corresponded to Pmin, and the largest positive effect corresponded to Alt; while the Weath (negative) and OM content (positive) had moderate effects.

The separate models for topsoils and subsoils showed a similar performance to that of the complete model (Figure A3). The model for topsoils accounted for 86% of the mercury variance (R^2 0.86, SRMR 0.07), and that of the subsoils accounted for 88% of the mercury variance (R^2 0.88, SRMR 0.08). Direct path coefficients to the Hg LV were quite similar in

both models, but the path coefficients of the interactions differed slightly between topsoils and subsoils. For subsoils, Alt showed a slightly lower effect on OM content and Weath, while OM content showed a larger effect on Weath and a lower effect on Pmin, when compared to topsoils. Interactions between predictor LVs explained a lower proportion of the variance of OM and Pmin, but a higher proportion of Weath in subsoils as compared to topsoils.

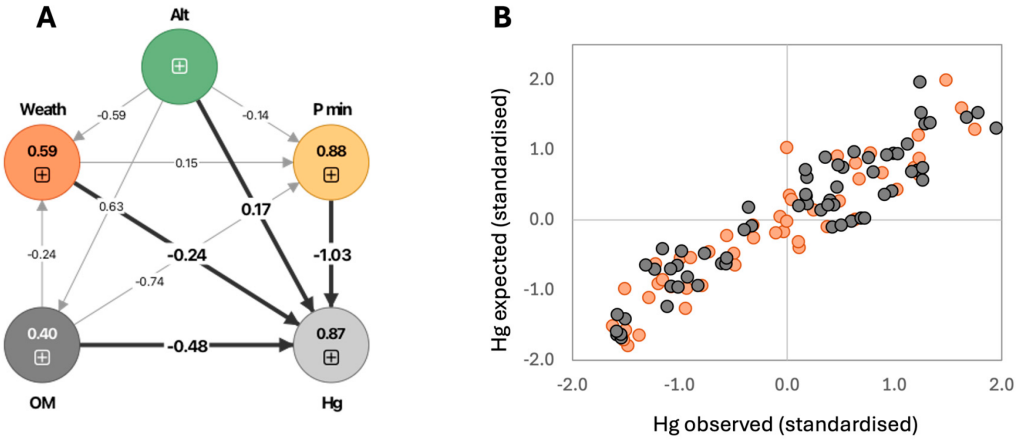


Figure 6. (**A**) Inner model of the mercury concentrations in the volcanic soils of Isla Santa Cruz, and (**B**) relationship between observed and expected (normalized) mercury concentrations. Response LV: Hg, mercury concentrations; predictor LVs: Alt, altitude; Pmin, primary minerals; Weath, chemical weathering; OM, organic matter. Bold numbers correspond to the direct path coefficients of the predictor LVs, and the other values correspond to the path coefficients related to the interactions between the predictor LVs. In (**B**), grey circles correspond to topsoil samples and orange circles correspond to subsoil samples.

4. Discussion

The soil pedogenetic processes of the Isla Santa Cruz have been extensively discussed and compared with those of other soils from volcanic areas in previous investigations [2,6–9,41,42]; the focus here is to discuss how the soil properties affect the mercury pool. Understanding the processes that govern the extensive mercury pool in volcanic soils is crucial to better predict how future climate, vegetation, and land-use changes might impact soil geochemistry and mercury dynamics.

4.1. Mercury in Santa Cruz Volcanic Soils: Content and Accumulation Mechanisms

The soils of Isla Santa Cruz are enriched in mercury, considering the threshold of 100 ng g^{-1} commonly applied to separate background and enriched soils [43]. Only seven topsoil samples and nine subsoil samples (11% and 17%, respectively) had concentrations lower than the background threshold, and almost all corresponded to soils of the AZ. In comparison, in an extensive study (>22,000 soil samples) on mercury content in topsoils of the European Union [44,45], 91% of the samples had mercury concentrations below 100 ng g^{-1}. In Isla Santa Cruz, mercury concentrations of soils from the AZ are within the upper quartile of this range, while those of soils from the other bioclimatic zones are in the upper 2% percentile of the values recorded in topsoils of the European Union.

To our knowledge, Peña-Rodríguez et al. [21] is the only comprehensive investigation on mercury content in volcanic soils. They analyzed 20 soils (94 samples) from seven European countries (EU: France, Greece, Hungary, Iceland, Italy, Portugal, and Spain). Almost half of the samples were also above the 100 ng g^{-1} threshold, and the range of values (5–635 ng g^{-1}) is comparable to that found in the present study. Considering the whole set of mercury measurements in volcanic soils (those of [21] and ours, N = 198), Isla

Santa Cruz soils have overall higher values: 44% of the samples from Santa Cruz were in the upper quartile (397–899 ng g^{-1}) but only 1% from the EU topsoils; in the second quartile (165–395 ng g^{-1}), the figures were 28% and 20%, respectively; in the third quartile (57–165 ng g^{-1}), they were 19% and 32%; and in the fourth quartile (5–56% ng g^{-1}), 9% and 46%, respectively. Despite this, high mercury concentrations were recorded in volcanic soils of Italy, up to 7450 ng g^{-1} [46].

Our results indicate that mercury concentrations in subsuperficial soil samples are highly correlated with those of the upper soil samples (Figure A1), suggesting mercury fluxes at the surface of the soil control mercury accumulation in the subsoil. Mercury was also correlated to altitude, iron content, and degree of chemical weathering. Correlation with iron was moderate (Figure 4, Table A1) but in line with those of previous investigations. Several investigations have already found correlations between mercury, organic matter, and Fe in soils [24,25,47–50]. It has been shown that mercury can strongly bind to sulphur groups [23,48,51–53], to nitrogen-containing compounds, and even to phenol and carbonyl groups [54–57] of the OM, and be adsorbed/coprecipitate with Fe oxides [58–62]. Although the OM MIR signal was of relatively moderate/low intensity, the correlation spectra for the topsoils and the subsoils showed highly significant correlations to OM functional groups (Figures A2 and 5): vibrations in the hydroxyl and aliphatic region (3500–2800 cm^{-1}) and the carbonyl/carboxylic/aromatic (1700–1550 cm^{-1}) region showed correlation coefficients larger than 0.75, suggesting their involvement in mercury binding in Isla Santa Cruz volcanic soils.

Mercury can also be adsorbed onto clay minerals, smectites being more efficient than kaolinite, gibbsite, and talc [24,63]. Despite the large abundance and diversity of clay minerals present in the volcanic soils of Isla Santa Cruz, their MIR absorbances were found to negatively correlate with mercury content. This indicates that, although they certainly can adsorb mercury, they exert a minor role in the mercury variations in these volcanic soils. In fact, soils from the AZ show large clay contents (Figure 3) but the lowest mercury concentrations in all bioclimatic zones.

4.2. Factors Affecting Mercury Spatial Distribution

The SEM models suggest that the main factors controlling mercury cycling in Isla Santa Cruz are the same across the soil compartments. No differences were found in the weights of the predictor LVs (path coefficients to Hg) between the complete and segregated models (Figure A1). Despite this, differences were observed in the coefficients of the interactions between predictors when comparing the segregated models: a higher proportion of the OM was explained in the topsoils, and a higher proportion of Weath (i.e., intensity of chemical weathering) in the subsoils. This is an expected result, given the large differences in vertical distribution of the OM between topsoils and subsoils, and indicates that OM is the main governing factor in the topsoils, while chemical weathering is more important in the subsoils.

The complete SEM model suggests that the content in Pmin (i.e., unweathered minerals) and Alt (altitude) have the largest controls on mercury content (Figure 7). The effect of altitude is positive but non-linear, as mercury concentration increases from the AZ to the SZ but flattens at the BZ. This may be due to a depletion of atmospheric mercury with increasing precipitation with altitude and the formation of a permanent fog layer at about 250 m of elevation, as described in Rial et al. [10]. Increases with altitude have also been observed in previous investigations of mercury accumulation in soils in altitudinal gradients [64], sometimes modulated by the formation of cloud layers [65]. Altitudinal differences control the spatial distribution of the bioclimatic zones defined here and in previous studies and, consequently, are associated with marked differences in vegetation

composition. These vegetation differences may, in turn, influence mercury accumulation and cycling in soils. Several investigations have shown that gaseous elemental mercury is taken up by vegetation and subsequently transferred to the soil, predominantly through litterfall [66–71], with soil mercury concentrations strongly correlated with mercury concentrations in litterfall [72]. In fact, mercury deposition through litterfall is considered the largest source of mercury to forest soils, although the deposition fluxes decrease from tropical to boreal areas [73]. This effect is more pronounced in topsoils compared to subsoils, where mercury content is more dependent on OM content and other soil properties [74].

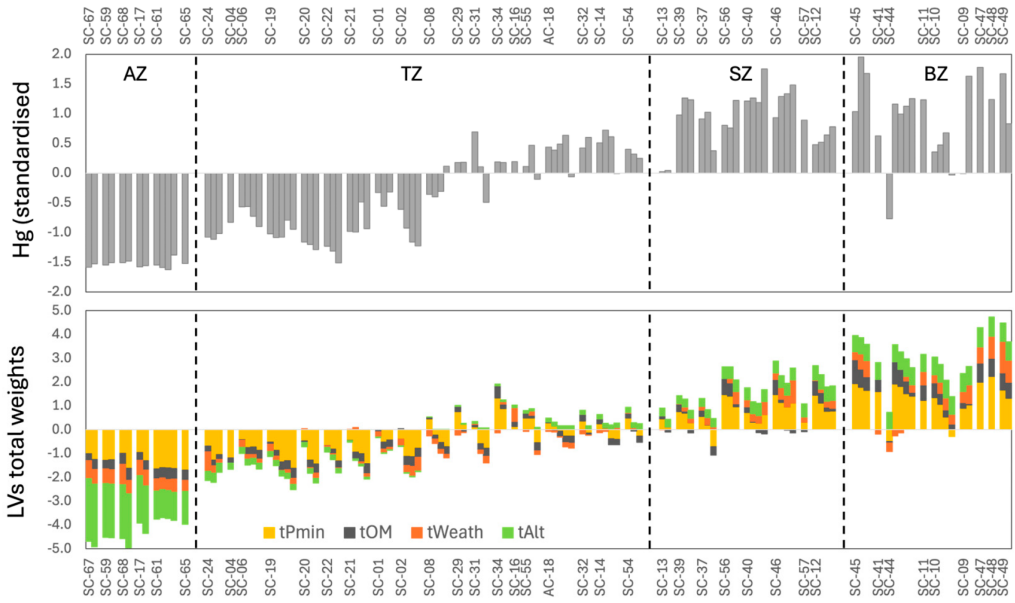


Figure 7. Standardized mercury concentrations and total weights of the drivers retained in the complete SEM model accounting for 87% of the mercury variance in topsoil and subsoil samples of Isla Santa Cruz. In each soil, samples from left to right are in depth order. Bioclimatic zones: AZ, arid zone; TZ, transition zone; SZ, Scalesia zone; BZ, brown zone (after [34,35]).

The effect of Pmin (primary minerals) is linear, and it probably accounts for a relative dissolution effect, as the wavenumbers retained in the SEM model correspond to olivine and pyroxene minerals. A study of mercury in the topsoil horizons of European volcanic soils revealed varying contributions of lithogenic mercury (i.e., Hg derived from the weathering of volcanic parent material) to total soil mercury [21]. In contrast, Grimaldi et al. [24] found much less variability in mercury content in highly weathered soils (volcanogenic parent material) in Oxisols and Ultisols in French Guiana, whilst also observing that lithogenic mercury becomes enriched as weathering progressed, pointing toward the fact that weathering simultaneously controls long-term mercury and mineralogical composition of these soils. In Isla Santa Cruz, soil mercury concentrations linearly decrease with increasing absorbance of primary minerals (olivines and pyroxenes, Figure A2), suggesting that for these soils the lithogenic mercury is negligible.

Weath (chemical weathering) and OM showed opposite, moderate weights. The negative sign of the Weath path coefficient is due to the fact that the STI values decrease as the chemical weathering intensity increases (STI and Fe loadings have opposite signs in Weath), so the overall effect is an increase in mercury content as the degree of weathering increases. Strong weathering in volcanic soils produce a large amount of highly reactive secondary phases (both crystalline and of low crystallinity) [6,9,41], with a large capacity to bind mercury—as described in the previous section.

The positive sign of OM indicates that it contributes to increasing mercury content (Figure A2). The MIR bands retained in the model correspond to aliphatic (methyl and

methene), carbonyl, carboxylic, and aromatic bonds, suggesting these are the most active in mercury accumulation in the Isla Santa Cruz soils. Thus, the SEM model captured the significant role of OM in mercury accumulation in volcanic soils.

Our results also point to interesting changes in the vertical distribution of mercury in the soils. In AZ, there is no vertical differentiation between soil compartments, and all factors show a similar distribution of weights. The low altitude is the main control, followed by Pmin. In TZ soils, Pmin and Weath become progressively more important, their effects varying with depth until the middle of the zone. In the second half of TZ, the effects turn to be positive, in topsoils in particular, showing Alt a weak contribution. This trend levels out in SZ soils, although vertical differentiation is not as clear as that of TZ soil located at lower elevations. In the BZ soils, all the effects increase, and the vertical differentiation is again evident. In many investigations, mercury content shows a significant decrease with depth [24,25,48,69,75,76], but in volcanic soils sedimentary discontinuities due to volcanic events result in complex mercury depth distribution profiles [21].

4.3. Land-Use Changes: Implications for the Mercury Cycling in Santa Cruz Soils

Land-use transformations have been shown to affect mercury cycling in forest soils. Transformation from native forests to grassland or agricultural land use significantly increases mercury mobility [77–81], due to a cascade of changes that affect mercury uptake by vegetation, soil organic matter content and molecular composition [82], and, in volcanic soils, changes in the evolution of the mineral phases and soil properties (e.g., [83]). As indicated before, litterfall is the main mercury flux to soils and different plant species contribute to different extents [64,74]. At a global scale, Wang et al. [84] estimated that tropical/subtropical forests contribute to 32% of the total mercury storage, temperate/boreal forests to 23%, grassland and steppe shrubland 28%, tundra by 7%, and desert and arid shrubland 10%. Fires, which are more frequent in human managed areas, pose an additional risk to mercury mobilization [85]. Wildfires were found to decrease mercury content by 88% in O horizons and up to 50% in the mineral soil [81].

The windward slopes of Isla Santa Cruz have been extensively transformed, as shown in a recent study by Herrera et al. [29]. In their work on the history of land cover in Isla Santa Cruz, these authors found that 94% of the non-protected area was covered by native vegetation in 1961 but decreased to 7% in 2018, due to clearing for agricultural expansion (67% of the area is covered with agricultural land and 26% by invasive species). Based on what has been outlined above, this implies that major changes to the factors controlling mercury cycling in the Santa Cruz soils already have occurred, with potential releases of mercury from the topsoils and altered atmospheric elemental mercury uptake linked to vegetation shifts. The extent of these effects and whether only topsoils were affected and subsoils remained undistributed is still to be established. Our study provides a unique, pre-transformation evaluation of mercury content and cycling that can serve as a reference state for comparing post-transformation conditions.

5. Conclusions

Mercury concentrations in the studied volcanic soils of Isla de Santa Cruz (Galapagos, Ecuador), collected in 1962, showed a large range of variation—19-fold (36–679 ng g^{-1})—and increased almost linearly with altitude. Differences between bioclimatic zones were highly significant. Concentrations at increasing depth in the soil were correlated to those of the uppermost layer, implying that mercury fluxes at the soil surface (most likely dominated by litterfall additions) controlled mercury accumulation in the subsoils. In agreement with previous investigations, mercury was found to be correlated with iron, organic matter content and quality (availability of aliphatic, carbonyl, carboxylic, and aromatic bonds), and degree

of chemical weathering of the soil. These facts suggest that soil pedogenetic evolution also played an important role in mercury accumulation. This assumption was reinforced by the results of the structural equation modeling (SEM), which suggested that altitude (positive) and the abundance of primary minerals (negative) had the largest controls on soil mercury content. Altitude, in the windward slopes of the island, integrates several environmental factors such as precipitation, temperature, vegetation communities, etc., all of which have been previously found to be involved in soil mercury cycling. The abundance of primary minerals is related to the degree of chemical weathering and soil pedogenesis.

Since this study was conducted on archived soil samples, our results and models approximate the factors involved in soil mercury accumulation prior to the extensive land-use transformations undergone in the windward areas of Isla Santa Cruz. Major changes in the factors controlling mercury cycling (soil properties, pedogenetic evolution, and vegetation composition) have certainly occurred since then, which may have resulted in increased releases of mercury to the atmosphere and waters, posing unconstrained threats to Isla Santa Cruz ecosystems today and in the future.

Supplementary Materials: The following supporting information can be downloaded at https://www.mdpi.com/article/10.3390/land15101920/s1. File: MIR-absorbances.xls, containing standardized absorbance intensities of the wavenumbers used for the structural equation modeling (SEM).

Author Contributions: Conceptualization, A.M.C., and O.L.-C.; methodology, A.M.C., M.T., and A.F.-G.; formal analysis, A.M.C.; investigation, A.M.C., A.F.-G., M.T., J.K.S., and O.L.-C.; resources, A.M.C. and O.L.-C.; data curation, A.M.C., O.L.-C. and A.F.-G.; writing—original draft preparation, A.M.C., A.F.-G., M.T., J.K.S., and O.L.-C.; writing—review and editing, A.M.C., A.F.-G., M.T., J.K.S., and O.L.-C.; visualization, A.M.C., O.L.-C.; funding acquisition, A.M.C., O.L.-C. All authors have read and agreed to the published version of the manuscript.

Funding: This research was funded by Xunta de Galicia—Grupos de Referencia Competitiva (ED431C 2025/018), and Convenio de colaboración (2024-CP070)—and ERC Consolidator Grant, PollutedPast (n 101087832). Views and opinions expressed are, however, those of the author(s) only and do not necessarily reflect those of the European Union or the European Research Council. Neither the European Union nor the granting authority can be held responsible for them.

Data Availability Statement: Data used for this investigation can be found in Appendix A and Supplementary Materials of this paper, and in the Supplementary Materials of the previous publication referenced in the text (Section 2.2).

Acknowledgments: The soil samples were donated to us by the late Georges Stoops, to whom we will always be deeply grateful. The authors are grateful to all PollutedPast team members for their support. We thank Cruz Ferro Vázquez for helping Stoops to sub-sample in his lab.

Conflicts of Interest: The authors declare no conflicts of interest. The funders had no role in the design of this study; in the collection, analyses, or interpretation of data; in the writing of the manuscript; or in the decision to publish the results.

Abbreviations

The following abbreviations are used in this manuscript:

SEM	Structural equation modeling
AZ	Arid Zone
TZ	Transition zone
SZ	Scalesia zone
BZ	Brown zone
OM	Organic matter
FTIR	Fourier Transform Infrared
ATR	Attenuated Total Reflectance

MIR Mid infrared
STI Silica–titania index
WIP Weathering index of Parker

Appendix A

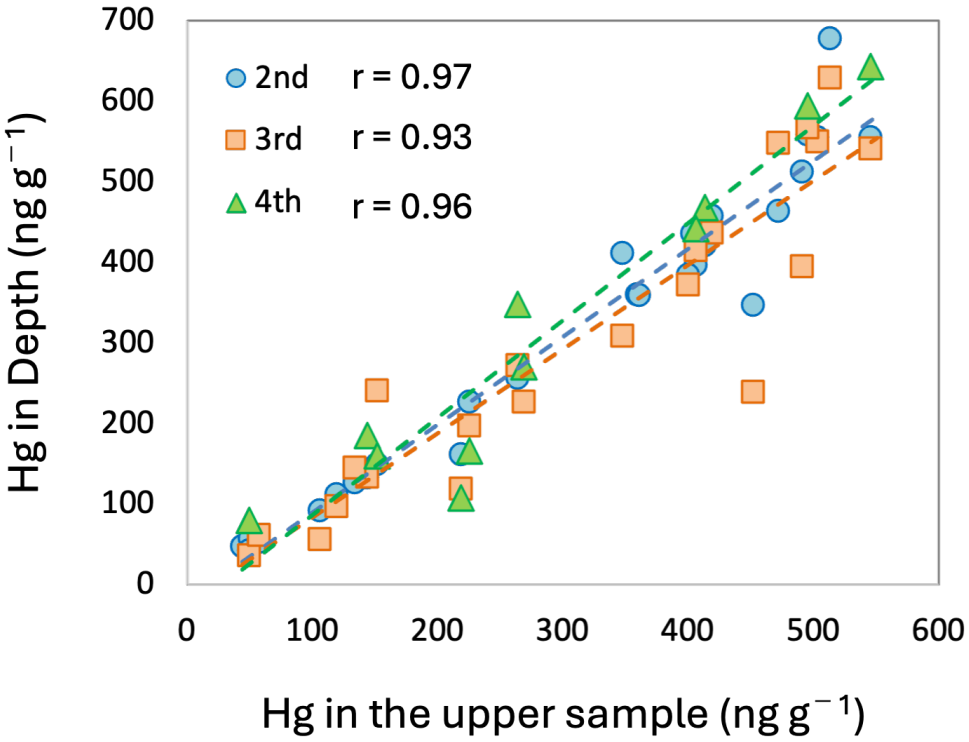


Figure A1. Correlation between mercury concentrations in the upper soil sample and samples taken at increasing depth.

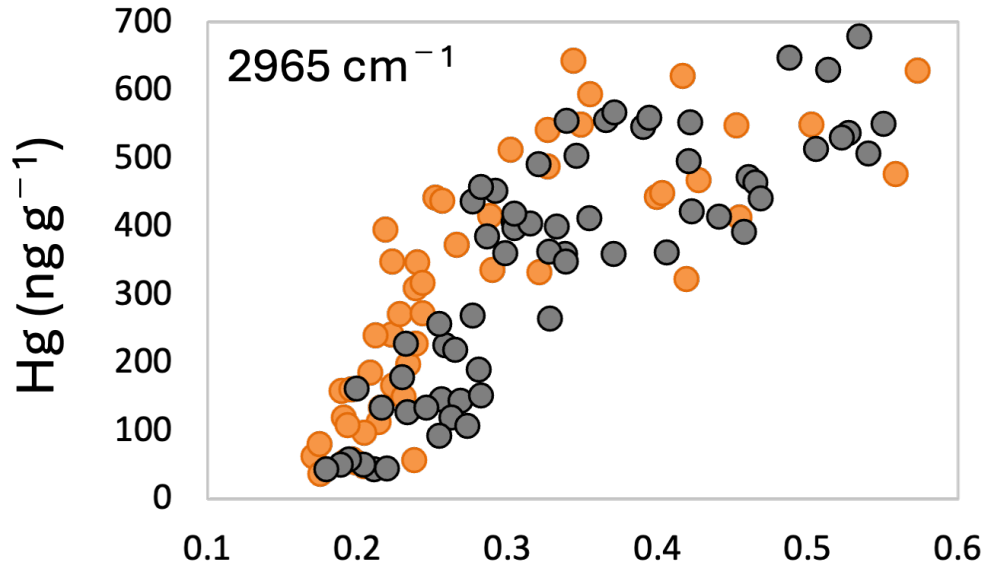


Figure A2. *Cont.*

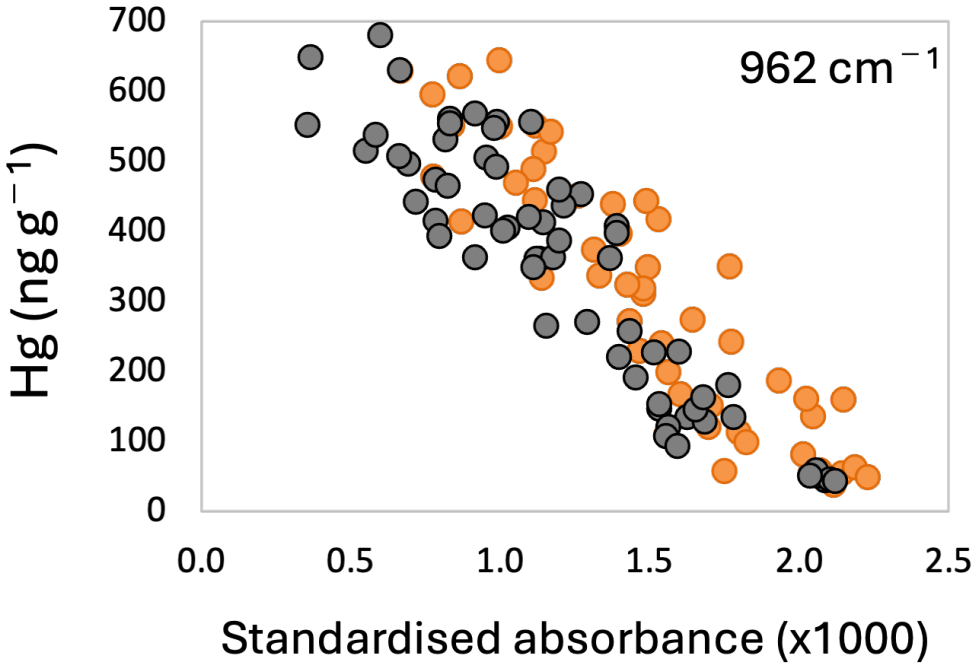


Figure A2. MIR absorbances showing the highest positive (methyl groups) and negative correlations (primary minerals, i.e., pyroxenes) to mercury concentrations. Grey circles correspond to topsoil samples and orange circles correspond to subsoil samples.

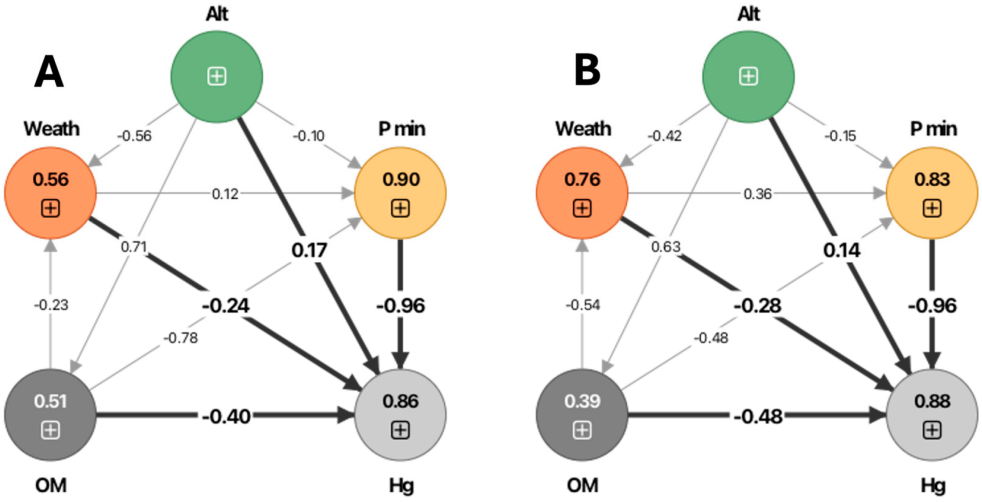


Figure A3. Segregated SEM models for (**A**) topsoils and (**B**) subsoils. Response LV: Hg, mercury concentrations; predictor LVs: Alt, altitude; P min, primary minerals; Weath, chemical weathering; OM, organic matter. Bold numbers correspond to the direct path coefficients of the predictor LVs, and the other values correspond to the path coefficients related to the interactions between the predictor LVs.

Table A1. Main MIR absorbances of the minerals identified by FTIR-ATR. Assignments based on [86–99].

Mineral	Wavenumber (cm^{-1})
Olivine	Forsterite—984, 867, 835, 610, 520, 501, 474 Fayalite—1003, 942, 852, 823, 554, 499, 460
Pyrioxene	Augite—1065, 962, 908, 862, 766, 671, 633, 503, 467, 461 Diopside—1066, 960, 908, 860, 673, 633, 503, 463 Enstatite—1051, 1001, 972, 945, 922, 895, 872, 725, 688, 644, 534, 496, 442

Table A1. *Cont.*

Mineral	Wavenumber (cm^{-1})
Plagioclase	Albite—1150, 1100, 1030, 988, 787, 764, 745, 723, 650, 608, 588, 530, 476, 463 Anorthite—1140, 1096, 1075, 1022, 990, 914, 772, 756, 727, 685, 669, 621, 604, 581, 567, 538, 484
Quartz	1165, 1082, 1051, 963, 797, 779, 729, 694, 517, 455
KaoliniteHalloysite	3694, 3652, 3620, 1114, 1029, 1005, 998, 935, 910, 788, 751, 678, 645, 527, 460
Gibssite	3620, 2652, 2469, 3375, 1021, 972, 800, 751, 666, 559, 523
Montmorillonite	3630, 3526, 3469, 3375, 1021, 972, 800, 751, 666, 559, 523
Talc	3677, 1017, 670, 536, 464, 425

Table A2. Correlation (Pearson coefficient) between the variables used in this study.

Topsoil	Iron	WIP	STI	Hg
Altitude	0.42	−0.46	−0.60	0.85
Iron		−0.52	−0.20	0.43
WIP			0.26	−0.31
STI				−0.74
Subsoil				
Altitude	0.72	−0.53	−0.93	0.83
Iron		−0.77	−0.79	0.67
WIP			0.58	−0.47
STI				−0.80

References

1. Granda, L.; Choez, G. *Población y Migración en Galápagos*; Informe Galápagos 2011–2012; DPNG-CGREGE-FCD-GC: Puerto Ayora, Ecuador, 2013; pp. 44–51.
2. Lasso, L.; Espinosa, J. Soils from the Galapagos islands. In *The Soils of Ecuador*; Springer International Publishing: Cham, Switzerland, 2017; pp. 139–150.
3. Bristow, C.; Hoffstetter, R.; Feininger, T.; Hall, M. *Léxico Estratigráfico del Ecuador*; Centre National de la Recherche Scientifique: Paris, France, 1977.
4. Winckell, A. Los paisajes de las Islas Galápagos. In *Los Paisajes Naturales del Ecuador: Las Regiones y Paisajes del Ecuador*; Winckell, A., Zebrowski, C., Sourdat, M., Eds.; CEDIG—IPGH—IRD: Quito, Ecuador, 1997.
5. Huttel, C.; Winckell, A.; Pourrut, P.; Viennot, M.; Acosta, J.; Almeida, G.; Carvajal, A.; Loaiza, C. *Inventario Cartografico de los Recursos Naturales, Geomorfologia, Vegetacion, Hidricos, Ecologicos y Biofisicos de las islas Galapagos Ecuador*; PRONAREG—INGALA: Quito, Ecuador, 1989.
6. Stoops, G. A micromorphological evaluation of pedogenesis on Isla Santa Cruz (Galápagos). *Span. J. Soil Sci. SJSS* **2013**, *3*, 14–37. [CrossRef]
7. Stoops, G.; Mees, F.; Dumon, M.; Adhikari, R.; Van Ranst, E. Soils of the coastal and lower belt of Galápagos Islands—The case of Isla Santa Fé and Isla Santa Cruz. *Geoderma Reg.* **2022**, *29*, e00520. [CrossRef]
8. Taboada, T.; Rodríguez-Lado, L.; Ferro-Vázquez, C.; Stoops, G.; Martínez Cortizas, A. Chemical weathering in the volcanic soils of Isla Santa Cruz (Galápagos Islands, Ecuador). *Geoderma* **2016**, *261*, 160–168. [CrossRef]
9. Taboada, T.; Ferro-Vázquez, C.; Stoops, G.; Martínez-Cortizas, A.; Rodríguez-Flores, R.; Rodríguez-Lado, L. Secondary aluminium, iron and silica phases across a volcanic soil climosequence, Galápagos Islands. *Eur. J. Soil Sci.* **2019**, *70*, 540–549. [CrossRef]
10. Rial, M.; Martínez Cortizas, A.; Taboada, T.; Rodríguez-Lado, L. Soil organic carbon stocks in Santa Cruz Island, Galapagos, under different climate change scenarios. *CATENA* **2017**, *156*, 74–81. [CrossRef]
11. Candra, I.N.; Gerzabek, M.H.; Ottner, F.; Wriessnig, K.; Tintner, J.; Schmidt, G.; Rampazzo, N.; Zehetner, F. Soil formation and mineralogical changes on basaltic lava vs scoria along a hydroclimatic gradient on Santa Cruz Island, Galápagos. *CATENA* **2023**, *220*, 106696. [CrossRef]
12. Paque, R.; Alomia Herrera, I.; Dixon, J.L.; Molina, A.; Zehetner, F.; Vanacker, V. Constraining the Effect of Climate and Rock Porosity on Weathering Extent in the Volcanic Island of Santa Cruz (Galápagos, Ecuador). *J. Geophys. Res. Earth Surf.* **2024**, *129*, e2024JF007651. [CrossRef]

13. Gerzabek, M.H.; Poch, R.M.; Álvarez, D.; Ploszczanski, L.; Zehetner, F. Strong Differences in Pedogenesis on Lava Vs. Scoria Along a Hydroclimatic Gradient on Santa Cruz Island/Galápagos Archipelago (Ecuador)—Insights From Micromorphology. *Span. J. Soil Sci.* **2025**, *15*, 14219. [CrossRef]
14. Candra, I.N.; Gerzabek, M.H.; Ottner, F.; Wriessnig, K.; Tintner, J.; Schmidt, G.; Rechberger, M.V.; Rampazzo, N.; Zehetner, F. Soil development and mineral transformations along a one-million-year chronosequence on the Galápagos Islands. *Soil Sci. Soc. Am. J.* **2021**, *85*, 2077–2099. [CrossRef]
15. Gerzabek, M.H.; Rechberger, M.V.; Schmidt, G.; Wriessnig, K.; Zehetner, F. Soil organic carbon and fine particle stocks along a volcanic chrono- and elevation-sequence on the Galápagos archipelago/Ecuador. *Geoderma Reg.* **2022**, *29*, e00508. [CrossRef]
16. Gerzabek, M.H.; Stoops, G.; Ottner, F.; Wang, S.-L.; Huang, L.-S.; Zehetner, F. The evolution of soil microstructure and micromineralogy along a soil age gradient on the Galápagos Islands (Ecuador). *Geoderma Reg.* **2023**, *32*, e00609. [CrossRef]
17. Rechberger, M.V.; Roberti, D.; Phillips, A.; Zehetner, F.; Keiblinger, K.M.; Kandeler, E.; Gerzabek, M.H. Cadmium Retention and Microbial Response in Volcanic Soils Along Gradients of Soil Age and Climate on the Galápagos Islands. *J. Environ. Qual.* **2021**, *50*, 1233–1245. [CrossRef]
18. Rechberger, M.V.; Zehetner, F.; Candra, I.N.; Gerzabek, M.H. Impact of soil development on Cu sorption along gradients of soil age and moisture on the Galápagos Islands. *CATENA* **2020**, *189*, 104507. [CrossRef]
19. Ferrara, R.; Mazzolai, B.; Lanzillotta, E.; Nucaro, E.; Pirrone, N. Volcanoes as emission sources of atmospheric mercury in the Mediterranean basin. *Sci. Total Environ.* **2000**, *259*, 115–121. [CrossRef] [PubMed]
20. Pyle, D.M.; Mather, T.A. The importance of volcanic emissions for the global atmospheric mercury cycle. *Atmos. Environ.* **2003**, *37*, 5115–5124. [CrossRef]
21. Peña-Rodríguez, S.; Pontevedra-Pombal, X.; Fernández-Calviño, D.; Taboada, T.; Arias-Estévez, M.; Martínez-Cortizas, A.; Nóvoa-Muñoz, J.C.; García-Rodeja, E. Mercury content in volcanic soils across Europe and its relationship with soil properties. *J. Soils Sediments* **2012**, *12*, 542–555. [CrossRef]
22. Schwesig, D.; Matzner, E. Pools and fluxes of mercury and methylmercury in two forested catchments in Germany. *Sci. Total Environ.* **2000**, *260*, 213–223. [CrossRef] [PubMed]
23. Skyllberg, U.; Bloom, P.R.; Qian, J.; Lin, C.-M.; Bleam, W.F. Complexation of Mercury(II) in Soil Organic Matter: EXAFS Evidence for Linear Two-Coordination with Reduced Sulfur Groups. *Environ. Sci. Technol.* **2006**, *40*, 4174–4180. [CrossRef] [PubMed]
24. Grimaldi, C.; Grimaldi, M.; Guedron, S. Mercury distribution in tropical soil profiles related to origin of mercury and soil processes. *Sci. Total Environ.* **2008**, *401*, 121–129. [CrossRef] [PubMed]
25. Guedron, S.; Grangeon, S.; Lanson, B.; Grimaldi, M. Mercury speciation in a tropical soil association; Consequence of gold mining on Hg distribution in French Guiana. *Geoderma* **2009**, *153*, 331–346. [CrossRef]
26. Hissler, C.; Probst, J.-L. Impact of mercury atmospheric deposition on soils and streams in a mountainous catchment (Vosges, France) polluted by chlor-alkali industrial activity: The important trapping role of the organic matter. *Sci. Total Environ.* **2006**, *361*, 163–178. [CrossRef] [PubMed]
27. Kohlenberg, A.J.; Turetsky, M.R.; Thompson, D.K.; Branfireun, B.A.; Mitchell, C.P.J. Controls on boreal peat combustion and resulting emissions of carbon and mercury. *Environ. Res. Lett.* **2018**, *13*, 035005. [CrossRef]
28. Guo, W.; Liu, M.; Zhang, Q.; Deng, Y.; Chu, Z.; Qin, H.; Li, Y.; Liu, Y.-R.; Zhang, H.; Zhang, W.; et al. Warming-Induced Vegetation Greening May Aggravate Soil Mercury Levels Worldwide. *Environ. Sci. Technol.* **2024**, *58*, 15078–15089. [CrossRef] [PubMed]
29. Herrera, I.A.; Paque, R.; Maertens, M.; Vanacker, V. History of Land Cover Change on Santa Cruz Island, Galapagos. *Land* **2022**, *11*, 1017. [CrossRef]
30. White, W.M.; McBirney, A.R.; Duncan, R.A. Petrology and geochemistry of the Galápagos Islands: Portrait of a pathological mantle plume. *J. Geophys. Res. Solid Earth* **1993**, *98*, 19533–19563. [CrossRef]
31. Wilson, E.L.; Harpp, K.S.; Schwartz, D.M.; Van Kirk, R. The Geochemical Evolution of Santa Cruz Island, Galápagos Archipelago. *Front. Earth Sci.* **2022**, *10*, 845544. [CrossRef]
32. Adelinet, M.; Fortin, J.; d'Ozouville, N.; Violette, S. The relationship between hydrodynamic properties and weathering of soils derived from volcanic rocks, Galapagos Islands (Ecuador). *Environ. Geol.* **2008**, *56*, 45–58. [CrossRef]
33. Pryet, A.; Domínguez, C.; Tomai, P.F.; Chaumont, C.; d'Ozouville, N.; Villacís, M.; Violette, S. Quantification of cloud water interception along the windward slope of Santa Cruz Island, Galapagos (Ecuador). *Agric. For. Meteorol.* **2012**, *161*, 94–106. [CrossRef]
34. Laurelle, J. *Galápagos*; Natuurwtenchappelijk Tijdschrift: Gent, Belgium, 1967; Volume 47.
35. Laurelle, J. Study of a soil sequence in Isla Santa Cruz (Galápagos Archipiélago, Ecuador). In *Galápagos Scientific Project 1964*; University of California, Symp. Pap., Mimeographed: Berkeley, CA, USA, 1964.
36. Parker, A. An Index of Weathering for Silicate Rocks. *Geol. Mag.* **1970**, *107*, 501–504. [CrossRef]
37. Jayawardena, U.d.S.; Izawa, E. A new chemical index of weathering for metamorphic silicate rocks in tropical regions: A study from Sri Lanka. *Eng. Geol.* **1994**, *36*, 303–310. [CrossRef]

38. Navrátil, T.; Burns, D.A.; Nováková, T.; Kaňa, J.; Rohovec, J.; Roll, M.; Ettler, V. Stability of mercury concentration measurements in archived soil and peat samples. *Chemosphere* **2018**, *208*, 707–711. [CrossRef] [PubMed]
39. Demšar, J.; Zupan, B. Orange: Data mining fruitful and fun-a historical perspective. *Informatica* **2013**, *37*, 55.
40. Ringle, C.M.; Wende, S.; Becker, J.M. *SmartPLS 3*; SmartPLS GmbH: Boenningstedt, Germany, 2015.
41. Stoops, G. Soils and Paleosoils of the Galápagos Islands: What We Know and What We Don't Know, A Meta-Analysis. *Pac. Sci.* **2014**, *68*, 1–17. [CrossRef]
42. Lasso, L.; Espinosa, J. Suelos de las Islas Galápagos. In *Suelos del Ecuador, Clasificación, uso y Manejo*; Espinosa, J., Moreno, J., Bernal, G., Eds.; Instituto Geográfico Militar: Quito, Ecuador, 2022; pp. 191–209.
43. Gustin, M.S.; Lindberg, S.E.; Weisberg, P.J. An update on the natural sources and sinks of atmospheric mercury. *Appl. Geochem.* **2008**, *23*, 482–493. [CrossRef]
44. Ballabio, C.; Jiskra, M.; Osterwalder, S.; Borrelli, P.; Montanarella, L.; Panagos, P. A spatial assessment of mercury content in the European Union topsoil. *Sci. Total Environ.* **2021**, *769*, 144755. [CrossRef] [PubMed]
45. Panagos, P.; Jiskra, M.; Borrelli, P.; Liakos, L.; Ballabio, C. Mercury in European topsoils: Anthropogenic sources, stocks and fluxes. *Environ. Res.* **2021**, *201*, 111556. [CrossRef] [PubMed]
46. Kabata-Pendias, A. *Trace Elements in Soils and Plants*; CRC Press; Taylor & Francis Group: Boca Raton, FL, USA, 2010.
47. Roulet, M.; Lucotte, M.; Saint-Aubin, A.; Tran, S.; Rhéault, I.; Farella, N.; De Jesus Da silva, E.; Dezencourt, J.; Sousa Passos, C.J.; Santos Soares, G.; et al. The geochemistry of mercury in central Amazonian soils developed on the Alter-do-Chão formation of the lower Tapajós River Valley, Pará state, Brazil. *Sci. Total Environ.* **1998**, *223*, 1–24. [CrossRef] [PubMed]
48. Palmieri, H.E.L.; Nalini, H.A.; Leonel, L.V.; Windmöller, C.C.; Santos, R.C.; de Brito, W. Quantification and speciation of mercury in soils from the Tripuí Ecological Station, Minas Gerais, Brazil. *Sci. Total Environ.* **2006**, *368*, 69–78. [CrossRef] [PubMed]
49. Nóvoa-Muñoz, J.C.; Pontevedra-Pombal, X.; Martínez-Cortizas, A.; García-Rodeja Gayoso, E. Mercury accumulation in upland acid forest ecosystems nearby a coal-fired power-plant in Southwest Europe (Galicia, NW Spain). *Sci. Total Environ.* **2008**, *394*, 303–312. [CrossRef] [PubMed]
50. Giesler, R.; Clemmensen, K.E.; Wardle, D.A.; Klaminder, J.; Bindler, R. Boreal Forests Sequester Large Amounts of Mercury over Millennial Time Scales in the Absence of Wildfire. *Environ. Sci. Technol.* **2017**, *51*, 2621–2627. [CrossRef] [PubMed]
51. Haitzer, M.; Aiken, G.R.; Ryan, J.N. Binding of Mercury(II) to Aquatic Humic Substances: Influence of pH and Source of Humic Substances. *Environ. Sci. Technol.* **2003**, *37*, 2436–2441. [CrossRef] [PubMed]
52. Gabriel, M.C.; Williamson, D.G. Principal Biogeochemical Factors Affecting the Speciation And Transport of Mercury through the terrestrial environment. *Environ. Geochem. Health* **2004**, *26*, 421–434. [CrossRef] [PubMed]
53. Galloway, J.M.; Parsons, M.B.; Ardakani, O.H.; Falck, H.; Fewster, R.E.; Swindles, G.T.; Sanei, H.; Palmer, M.J.; Nasser, N.A.; Patterson, R.T. Organic matter is a predominant control on total mercury concentration of near-surface lake sediments across a boreal to low Arctic tundra transect in northern Canada. *Sci. Total Environ.* **2024**, *954*, 176466. [CrossRef] [PubMed]
54. Nieboer, E.; Richardson, D.H.S. The replacement of the nondescript term 'heavy metals' by a biologically and chemically significant classification of metal ions. *Environ. Pollut. Ser. B Chem. Phys.* **1980**, *1*, 3–26. [CrossRef]
55. Drexel, R.T.; Haitzer, M.; Ryan, J.N.; Aiken, G.R.; Nagy, K.L. Mercury(II) Sorption to Two Florida Everglades Peats: Evidence for Strong and Weak Binding and Competition by Dissolved Organic Matter Released from the Peat. *Environ. Sci. Technol.* **2002**, *36*, 4058–4064. [CrossRef] [PubMed]
56. Bulgariu, L.; Ratoi, M.; Bulgariu, D.; Macoveanu, M. Adsorption potential of mercury(II) from aqueous solutions onto Romanian peat moss. *J. Environ. Sci. Health Part A* **2009**, *44*, 700–706. [CrossRef] [PubMed]
57. Luo, H.; Cheng, Q.; Fan, Q.; He, D.; Wang, X.; Sun, J.; Li, J.; Pan, X. FT-IR and synchronous fluorescence two-dimensional correlation spectroscopic analysis on the binding properties of mercury onto humic acids as influenced by pH modification and sulfide addition. *Sci. Total Environ.* **2022**, *819*, 152047. [CrossRef] [PubMed]
58. Asmund, G.; Nielsen, S.P. Mercury in dated Greenland marine sediments. *Sci. Total Environ.* **2000**, *245*, 61–72. [CrossRef] [PubMed]
59. Fitzgerald, W.F.; Lamborg, C.H.; Hammerschmidt, C.R. Marine Biogeochemical Cycling of Mercury. *Chem. Rev.* **2007**, *107*, 641–662. [CrossRef] [PubMed]
60. Richard, J.-H.; Bischoff, C.; Ahrens, C.G.M.; Biester, H. Mercury (II) reduction and co-precipitation of metallic mercury on hydrous ferric oxide in contaminated groundwater. *Sci. Total Environ.* **2016**, *539*, 36–44. [CrossRef] [PubMed]
61. Nawab, J.; Ghani, J.; Rehman, S.A.U.; Idress, M.; Luqman, M.; Khan, S.; Asghar, A.; Rahman, Z. Biomonitoring of mercury in water, sediments, and fish (brown and rainbow trout) from remote alpine lakes located in the Himalayas, Pakistan. *Environ. Sci. Pollut. Res.* **2022**, *29*, 81021–81036. [CrossRef] [PubMed]
62. Qu, R.; Han, G.; Liu, M.; Yang, K.; Li, X.; Liu, J. Fe, Rather Than Soil Organic Matter, as a Controlling Factor of Hg Distribution in Subsurface Forest Soil in an Iron Mining Area. *Int. J. Environ. Res. Public Health* **2020**, *17*, 359. [CrossRef] [PubMed]
63. Weerasooriya, R.; Tobschall, H.J.; Seneviratne, W.; Bandara, A. Transition state kinetics of Hg(II) adsorption at gibbsite–water interface. *J. Hazard. Mater.* **2007**, *147*, 971–978. [CrossRef] [PubMed]

64. Blackwell, B.D.; Driscoll, C.T. Deposition of Mercury in Forests along a Montane Elevation Gradient. *Environ. Sci. Technol.* **2015**, *49*, 5363–5370. [CrossRef] [PubMed]
65. Stankwitz, C.; Kaste, J.M.; Friedland, A.J. Threshold Increases in Soil Lead and Mercury from Tropospheric Deposition Across an Elevational Gradient. *Environ. Sci. Technol.* **2012**, *46*, 8061–8068. [CrossRef] [PubMed]
66. Mélières, M.-A.; Pourchet, M.; Charles-Dominique, P.; Gaucher, P. Mercury in canopy leaves of French Guiana in remote areas. *Sci. Total Environ.* **2003**, *311*, 261–267. [CrossRef] [PubMed]
67. Obrist, D.; Johnson, D.W.; Lindberg, S.E.; Luo, Y.; Hararuk, O.; Bracho, R.; Battles, J.J.; Dail, D.B.; Edmonds, R.L.; Monson, R.K.; et al. Mercury Distribution Across 14 U.S. Forests. Part I: Spatial Patterns of Concentrations in Biomass, Litter, and Soils. *Environ. Sci. Technol.* **2011**, *45*, 3974–3981. [CrossRef] [PubMed]
68. Enrico, M.; Roux, G.l.L.; Marusczak, N.; Heimbürger, L.-E.; Claustres, A.; Fu, X.; Sun, R.; Sonke, J.E. Atmospheric Mercury Transfer to Peat Bogs Dominated by Gaseous Elemental Mercury Dry Deposition. *Environ. Sci. Technol.* **2016**, *50*, 2405–2412. [CrossRef] [PubMed]
69. Wang, X.; Luo, J.; Yin, R.; Yuan, W.; Lin, C.-J.; Sommar, J.; Feng, X.; Wang, H.; Lin, C. Using Mercury Isotopes To Understand Mercury Accumulation in the Montane Forest Floor of the Eastern Tibetan Plateau. *Environ. Sci. Technol.* **2016**, *51*, 801–809. [CrossRef] [PubMed]
70. Zhou, J.; Obrist, D. Global Mercury Assimilation by Vegetation. *Environ. Sci. Technol.* **2021**, *55*, 14245–14257. [CrossRef] [PubMed]
71. Méndez-López, M.; Gómez-Armesto, A.; Alonso-Vega, F.; Pontevedra-Pombal, X.; Fonseca, F.; de Figueiredo, T.; Arias-Estévez, M.; Nóvoa-Muñoz, J.C. The role of afforestation species as a driver of Hg accumulation in organic horizons of forest soils from a Mediterranean mountain area in SW Europe. *Sci. Total Environ.* **2022**, *827*, 154345. [CrossRef] [PubMed]
72. Luo, Y.; Duan, L.; Wang, L.; Xu, G.; Wang, S.; Hao, J. Mercury concentrations in forest soils and stream waters in northeast and south China. *Sci. Total Environ.* **2014**, *496*, 714–720. [CrossRef] [PubMed]
73. Wang, X.; Bao, Z.; Lin, C.-J.; Yuan, W.; Feng, X. Assessment of Global Mercury Deposition through Litterfall. *Environ. Sci. Technol.* **2016**, *50*, 8548–8557. [CrossRef] [PubMed]
74. Gruba, P.; Socha, J.; Pietrzykowski, M.; Pasichnyk, D. Tree species affects the concentration of total mercury (Hg) in forest soils: Evidence from a forest soil inventory in Poland. *Sci. Total Environ.* **2019**, *647*, 141–148. [CrossRef] [PubMed]
75. Guédron, S.; Grangeon, S.; Jouravel, G.; Charlet, L.; Sarret, G. Atmospheric mercury incorporation in soils of an area impacted by a chlor-alkali plant (Grenoble, France): Contribution of canopy uptake. *Sci. Total Environ.* **2013**, *445–446*, 356–364. [CrossRef] [PubMed]
76. Obrist, D.; Pokharel, A.K.; Moore, C. Vertical Profile Measurements of Soil Air Suggest Immobilization of Gaseous Elemental Mercury in Mineral Soil. *Environ. Sci. Technol.* **2014**, *48*, 2242–2252. [CrossRef] [PubMed]
77. Porvari, P.; Verta, M.; Munthe, J.; Haapanen, M. Forestry Practices Increase Mercury and Methyl Mercury Output from Boreal Forest Catchments. *Environ. Sci. Technol.* **2003**, *37*, 2389–2393. [CrossRef] [PubMed]
78. Mainville, N.; Webb, J.; Lucotte, M.; Davidson, R.; Betancourt, O.; Cueva, E.; Mergler, D. Decrease of soil fertility and release of mercury following deforestation in the Andean Amazon, Napo River Valley, Ecuador. *Sci. Total Environ.* **2006**, *368*, 88–98. [CrossRef] [PubMed]
79. Eklöf, K.; Schelker, J.; Sørensen, R.; Meili, M.; Laudon, H.; von Brömssen, C.; Bishop, K. Impact of Forestry on Total and Methyl-Mercury in Surface Waters: Distinguishing Effects of Logging and Site Preparation. *Environ. Sci. Technol.* **2014**, *48*, 4690–4698. [CrossRef] [PubMed]
80. Gamby, R.L.; Hammerschmidt, C.R.; Costello, D.M.; Lamborg, C.H.; Runkle, J.R. Deforestation and cultivation mobilize mercury from topsoil. *Sci. Total Environ.* **2015**, *532*, 467–473. [CrossRef] [PubMed]
81. Homann, P.S.; Darbyshire, R.L.; Bormann, B.T.; Morrissette, B.A. Forest Structure Affects Soil Mercury Losses in the Presence and Absence of Wildfire. *Environ. Sci. Technol.* **2015**, *49*, 12714–12722. [CrossRef] [PubMed]
82. Verde, J.R.; Buurman, P.; Martínez-Cortizas, A.; Macías, F.; Camps Arbestain, M. NaOH-extractable organic matter of andic soils from Galicia (NW Spain) under different land use regimes: A pyrolysis GC/MS study. *Eur. J. Soil Sci.* **2008**, *59*, 1096–1110. [CrossRef]
83. Farella, N.; Lucotte, M.; Davidson, R.; Daigle, S. Mercury release from deforested soils triggered by base cation enrichment. *Sci. Total Environ.* **2006**, *368*, 19–29. [CrossRef] [PubMed]
84. Wang, X.; Yuan, W.; Lin, C.-J.; Zhang, L.; Zhang, H.; Feng, X. Climate and Vegetation As Primary Drivers for Global Mercury Storage in Surface Soil. *Environ. Sci. Technol.* **2019**, *53*, 10665–10675. [CrossRef] [PubMed]
85. Turetsky, M.R.; Harden, J.W.; Friedli, H.R.; Flannigan, M.; Payne, N.; Crock, J.; Radke, L. Wildfires threaten mercury stocks in northern soils. *Geophys. Res. Lett.* **2006**, *33*, 175572. [CrossRef]
86. Jozanikohan, G.; Abarghooei, M.N. The Fourier transform infrared spectroscopy (FTIR) analysis for the clay mineralogy studies in a clastic reservoir. *J. Pet. Explor. Prod. Technol.* **2022**, *12*, 2093–2106. [CrossRef]
87. Koike, C.; Chihara, H.; Tsuchiyama, A.; Suto, H.; Sogawa, H.; Okuda, H. Compositional dependence of infrared absorption spectra of crystalline silicate. *Astron. Astrophys.* **2003**, *399*, 1101–1107. [CrossRef]

88. Kim, D.; Jung, H. Deformation microstructures of olivine and chlorite in chlorite peridotites from Almklovdalen in the Western Gneiss Region, southwest Norway, and implications for seismic anisotropy. *Int. Geol. Rev.* **2015**, *57*, 650–668. [CrossRef]
89. Lane, M.D.; Glotch, T.D.; Dyar, M.D.; Pieters, C.M.; Klima, R.; Hiroi, T.; Bishop, J.L.; Sunshine, J. Midinfrared spectroscopy of synthetic olivines: Thermal emission, specular and diffuse reflectance, and attenuated total reflectance studies of forsterite to fayalite. *J. Geophys. Res. Planets* **2011**, *116*, E08010. [CrossRef]
90. Grégoire, B.; Ferrage, E. Quantifying the Molecular Orientation and Distribution of Water Populations in Smectites: A Self-Consistent Framework Combining Polarized ATR-FTIR, XRD, and Molecular Simulations. *J. Phys. Chem. C* **2026**, *130*, 10637–10649. [CrossRef]
91. García-Vicente, A.; Lorenzo, A.; Morales, J.; García-Romero, E.; Suárez, M. Field Spectroscopy Applied to the Kaolinite Polytypes Identification. *Environ. Sci. Proc.* **2021**, *6*, 16. [CrossRef]
92. Du Plessis, P.I.; Gazley, M.F.; Tay, S.L.; Trunfull, E.F.; Knorsch, M.; Branch, T.; Fourie, L.F. Quantification of Kaolinite and Halloysite Using Machine Learning from FTIR, XRF, and Brightness Data. *Minerals* **2021**, *11*, 1350. [CrossRef]
93. Caccamo, M.T.; Mavilia, G.; Mavilia, L.; Lombardo, D.; Magazù, S. Self-Assembly Processes in Hydrated Montmorillonite by FTIR Investigations. *Materials* **2020**, *13*, 1100. [CrossRef] [PubMed]
94. Balan, E.; Paulatto, L.; Liu, J.; Ingrin, J. Low-temperature infrared spectrum and atomic-scale structure of hydrous defects in diopside. *Eur. J. Mineral.* **2020**, *32*, 505–520. [CrossRef]
95. Madejová, J. FTIR techniques in clay mineral studies. *Vib. Spectrosc.* **2003**, *31*, 1–10. [CrossRef]
96. Peternella, W.S.; da Costa, A.C.S. Evaluation of a Toposequence of Soils Derived from Basalt by Fourier Transform Infrared Spectroscopy. *Open Access Libr. J.* **2021**, *8*, e7867.
97. Pinet, P.C.; Daydou, Y.H.; Chevrel, S.D. Olivine composition and reflectance spectroscopy relationship revisited from advanced MGM deconvolution based on synthetic and natural samples. *Icarus* **2022**, *373*, 114765. [CrossRef]
98. Pironon, J.; Pelletier, M.; De Donato, P.; Mosser-Ruck, R. Characterization of smectite and illite by FTIR spectroscopy of interlayer NH4+ cations. *Clay Miner.* **2003**, *38*, 201–211. [CrossRef]
99. Vahur, S.; Kiudorv, L.; Somelar, P.; Cayme, J.-M.; Retrato, M.D.C.; Remigio, R.J.; Sharma, V.; Oras, E.; Leito, I. Quantitative mineralogical analysis of clay-containing materials using ATR-FT-IR spectroscopy with PLS method. *Anal. Bioanal. Chem.* **2021**, *413*, 6535–6550. [CrossRef] [PubMed]

Disclaimer/Publisher's Note: The statements, opinions and data contained in all publications are solely those of the individual author(s) and contributor(s) and not of MDPI and/or the editor(s). MDPI and/or the editor(s) disclaim responsibility for any injury to people or property resulting from any ideas, methods, instructions or products referred to in the content.